Applied Catalysis B: Environmental 199 (2016) 485–493

Contents lists available at ScienceDirect

Applied Catalysis B: Environmental

journal homepage: www.elsevier.com/locate/apcatb

Role of chain length of the capping agents of iron oxide based fuel borne catalysts in the enhancement of soot combustion activity

Paweł Stelmachowski[a,*], Piotr Legutko[a], Anna Kopacz[a], Tomasz Jakubek[a], Paulina Indyka[a], Piotr Pietrzyk[a], Michał Wojtasik[b], Jarosław Markowski[b], Wojciech Krasodomski[b], Leszek Ziemiański[b], Grażyna Żak[b], Zbigniew Sojka[a], Andrzej Kotarba[a,*]

[a] Faculty of Chemistry, Jagiellonian University in Krakow, Ingardena 3, 30-060 Kraków, Poland
[b] Oil and Gas Institute—National Research Institute, Lubicz 25A, 31-503 Kraków, Poland

ARTICLE INFO

Article history:
Received 15 March 2016
Received in revised form 20 June 2016
Accepted 23 June 2016
Available online 24 June 2016

Keywords:
FBC
Soot combustion
Catalyst
Iron oxide
Fe_2O_3 nanoparticles

ABSTRACT

A series of fuel borne catalysts (FBC) based on an iron oxide core stabilized by various long chain carboxylic acids were synthesized, characterized and tested in model soot combustion. As the capping agents methacrylic (C4), undecylenic (C11), oleic (C18) and erucic (C22) acids were used. The FBC precursors and the resultant catalysts were examined by Raman, FTIR, EPR, UV–vis and TEM/SAED techniques, whereas the catalytic reactivity in combustion of a model soot (Printex U) was evaluated by TG/DTA. For all the investigated FBC derived catalysts, it was found that the core of the catalyst consists of Fe_2O_3 of a crystallite size in range of 5–8 nm, which is beneficial for the soot combustion activity. While a strong positive effect on the catalyst performance was observed for all the alkyl chain lengths, the best results were obtained for a hybrid FBC catalyst with two types (C11 and C18) of capping ligands. The effect of the chain length of the capping agent on the soot combustion process was discussed in terms of promotion of soot ignition by the more reactive C11 and combustion sustentation by heat transfer from the long chain C18 to soot particles, as implied by the observed overlapping of the combustion temperature windows of those moieties. For such hybrid catalysts, the ignition temperature of the soot combustion was lowered to almost 150 °C, and the total soot combustion accomplished below ~470 °C. The high activity of the hybrid FBC catalysts makes them a promising alternative/backup for the particulate filter technology in light oil burners and related applications.

0. Introduction

Among the urban air pollutants, the abatement of nanometric carbonaceous particular matter (PM) is recognized as one of the most important issues for environmental catalysis. The legal regulations limiting the emission of PM into the atmosphere are systematically tightened down to 4.5 mg/km for light passenger and commercial vehicles, with both spark and compression ignition (Euro6) [1]. Similar restrictions are applicable to PM emitted from stationary sources such as hydrocarbon burning. There are essentially two basic strategies for the mitigation of PM emission. The most widely used for mobile sources, especially powered by diesel fuel, is the application of DPF filters. The less explored approach involves in-situ formed fuel borne catalysts (FBC), which are used as additives to increase fuel efficiency and reduce harmful PM content in the exhaust gases [2–7]. Such solution is also applied to improve the combustion of light fuel oil in the domestic and industrial heat production burners. Undesired accumulation of soot in a burner and chimney ducts may severely decrease the ventilation efficiency or even cause hazard of an autogenous induced soot explosion.

The FBC catalyst, added in the form of an organometallic precursor, is composed of metal-oxo/hydroxo cores surrounded by organic capping ligands, constituted by long-chain carboxylic acids, which enable their suspension in the liquid fuel. More expensive and less popular FBC precursors are ferrocene and ferrous picrate [7–10]. Although the details of the PM oxidation mechanism in the presence of the FBC catalysts are difficult to elucidate due to severe reaction conditions and low residence time in the

* Corresponding authors.
E-mail addresses: pawel.stelmachowski@uj.edu.pl (P. Stelmachowski), kotarba@chemia.uj.edu.pl (A. Kotarba).

http://dx.doi.org/10.1016/j.apcatb.2016.06.056
0926-3373/

Table 1
A summary of iron oxide/hydroxide core stabilizers and sample designations.

Carboxylic acid stabilizer	Sample label	Iron content/wt.%	Mass loss upon heating @ 750 °C/%
methacrylic acid	FBC-C4	3.8	16
undecylenic acid	FBC-C11	3.7	30
oleic acid	FBC-C18	14.1	19
eruic acid	FBC-C22	11.8	38
undecylenic and oleic acid (1:1)	FBC-(C11 + C18)	10.1	21

combustion chamber, there is a certain agreement in the literature concerning the principal reaction steps inferred from the dedicated model studies. They provide not only useful insights into the reaction mechanism but are also helpful for understanding the role of the FBC catalyst [11–15]. The catalytic PM combustion is an exothermic reaction, occurring at the heterogeneous triple point constituted by the FBC catalyst – soot particle – dioxygen interphase. It has been suggested that in the first stage of the reaction the metal oxide nanoparticles are produced by burning the organic shell and are adsorbed onto the surface of PM particles [3] or incorporated into them during soot formation [16]. This is followed by a redox reaction, wherein the metal is reduced to its lower oxidation state while promoting the PM oxidation. Because of the decreased stability of metals at low oxidation states in O_2 reach condition, their rapid oxidation occurs using the heat of the exhaust gases [16–18].

Typically, additives containing metal compounds (mainly oxides) used as catalysts for soot oxidation are based on transition metals [17,19] that exhibit the ability to form complexes, and undergo redox reactions readily, which is particularly important in facilitating the combustion process. Modern complexes, in comparison to the previous generation of the organometallic additives, do not form micelles containing inaccessible metal cations. Instead, by forming nanometer-sized metal oxide particles, they provide a high contact area between the soot and the catalyst, thereby lowering the soot ignition temperature efficiently [20]. The beneficial effect of the iron-oxide particle size was observed only below 20 nm [12].

The low price, environmental friendliness, high reactivity and susceptibility for facile surface and/or structural modifications brought iron oxide based materials (Fe_xO_y) to the spotlight as soot combustion catalysts. Various iron oxide based phases are catalytically active in soot oxidation, such as hematite [13–15], potassium ferrites [21,22] or iron oxide particles supported on alumina [23]. The importance of both surface and bulk oxygen transport in iron oxide nanocrystals is critical for the effective transfer of reactive oxygen from the catalyst to the soot, which is vital for the combustion process. The amorphous domains are supposed to be responsible for the surface oxygen diffusion, whereas the crystalline ones are responsible for bulk oxygen diffusion [24].

In the context of the in-situ transformation of the FBC catalyst into a fluidized, catalytically active form, an important issue is the chemical nature of capping ligands and their impact on the activity of the FBC catalyst nanoparticles in fuel combustion [2]. A variety of different organic acids is mentioned to be used for preventing particle aggregation and deposit formation, as described in patent literature. A detailed overview can be found in the Supplementary data. The declared organic acids are mostly cheap and available from natural sources, with the number of carbon atoms in the chain ranging from 10 to 50. In the case of oxide nanoparticles investigated in the context of size- and shape-controlled nanocrystal synthesis, oleic acid is one of the most widely employed stabilizers [25]. However, the function of the organic component in the soot combustion process has not been addressed as yet. It has been shown furthermore, that iron-oxide particles are more involved in the soot oxidation process, rather than in the early soot formation stage, as revealed by recent TEM studies [26]. Thus, in the model soot combustion laboratory tests of the FBC catalysts a model synthetic soot of defined composition and particle size distribution is used for screening their performance.

The aim of the study was to investigate the role of capping ligands of the iron-based FBC catalyst dedicated for light oil burners in the PM combustion process using a model soot. Although the applied conditions are different from the real ones of the burner, they reflect to a large extent the main features of the soot combustion process, as shown in our recent paper [12]. Therefore the obtain results provide a useful rational guidance for the optimization of the organic component of the FBC catalyst precursors.

1. Experimental

1.1. Materials

The FBC precursors were obtained in a three-step procedure through the stabilization of the iron hydroxy-oxides in an organic solvent. Firstly, the precipitates of iron hydroxy-oxides were obtained by ammonia addition to the solution of Fe(II) and Fe(III) sulfates (ferrous sulfate heptahydrate, purum, Chempur, cat. no. 529028406 and ferric sulfate hydrate, puriss p.a. Sigma-Aldrich, cat. no. 307718 salts were used). The precipitates were obtained at a temperature of 60 °C, by addition of ammonia until the pH was 8, followed by separation from the solution by filtering and subsequent washing. Chemical analysis showed no sulphur contamination of the final products.

Secondly, the precipitated iron compounds were added to the organic dispersant, which was a mixture of aromatic solvents (toluene and Shellsol D60®, provided by ShellChemicals, CAS no. 64742-48-9) and the carboxylic acid (used as a capping agent). To obtain a homogeneous suspension the solution was stirred at 80 °C for 5 h. The following capping agents were used for the FBC synthesis: methacrylic (C4), undecylenic (C11), oleic (C18), erucic (C22) and a 1:1 mixture of undecylenic and oleic acids (C11, C18). For all the prepared dispersants the ratio of the aromatic solvent to carboxylic acid was 10:1. In the third step, the residual Fe(II) present in the FBC precursors were transformed into Fe(III) via oxidation with 30% hydrogen peroxide at 50 °C for 1 h. It is worth mentioning that the resultant water can be easily removed after the reaction, which supports application of H_2O_2 as an oxidant. The products were separated by extraction in toluene and filtration using a pressure filtered with diatomaceous earth as a filter aid. The yields of the final product depended on the applied dispersant type and were within a range from 30 to 75 wt.%.

The list of all the investigated samples along with the labeling and iron content is presented in Table 1, along with a total mass loss due to the heating in the air up to 750 °C.

1.2. Methods

Determination of the iron content was performed by means of an optical emission spectrometer with inductively coupled plasma (ICP OES) SPECTRO ARCOS SOP in the wavelength range of 130–770 nm, allowing for simultaneous determination of all the elements (metals and nonmetals). The samples for analysis were

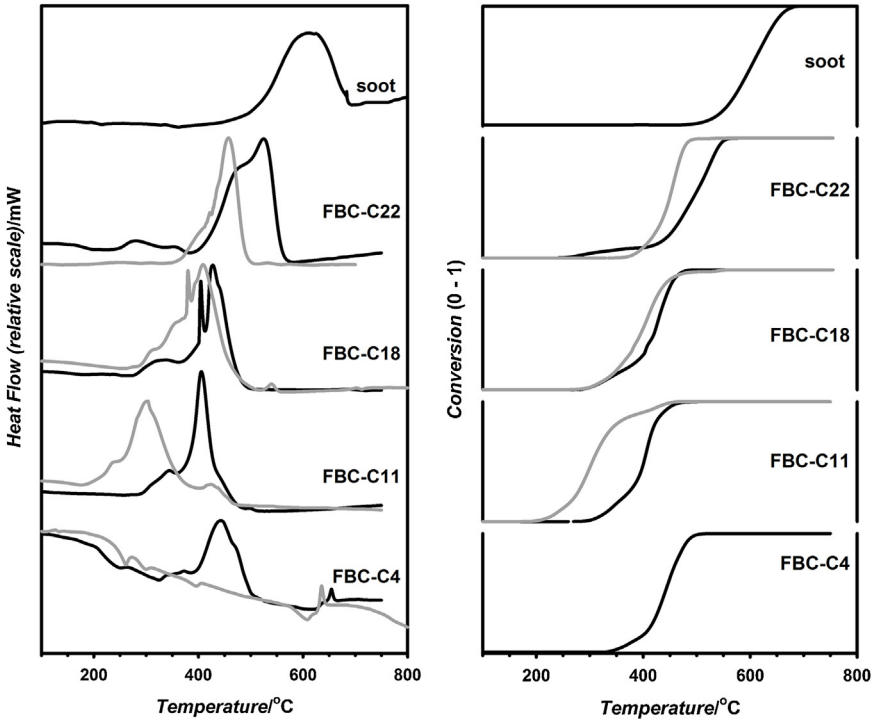

Fig. 1. Reactivity tests of soot combustion performed with the FBC-C4, FBC-C11, FBC-C18 and FBC-C22 precursors expressed as (A) DTA curves and (B) conversion type curves calculated from mass loss. Black lines: temperature programmed oxidation of soot (Printex U) in air atmosphere along with non-catalyzed Printex U oxidation. Grey lines: thermal decomposition (oxidation) of the FBC catalyst alone.

prepared by diluting in a high-purity naphtha, and the concentration was determined based on a calibration curve for the specific standards.

The Raman spectra were recorded at room temperature in the range of 150–800 cm^{-1} upon excitation with 785 nm laser beam with a Renishaw InVia spectrometer coupled with a confocal microscope Leica DMLM and CCD detector. At least nine scans for each sample were accumulated in order to provide a sufficient signal to noise ratio. The preparation of the samples for Raman analysis consisted in spraying of the diluted FBC precursor onto a quartz microscopic plate. Dilution and spraying were applied to prevent agglomeration of the iron oxide particles. For poorly crystallized materials – those without heat treatment – the Raman spectra were recorded for the material dispersed on the quartz plate. Additionally, in order to increase the intensity of the possible relevant bands, the scraped powder was piled in the cylindrical recess in the sample holder. The infrared spectra were taken using an FT-IR spectrometer Nicolet IR200 with a single reflection ATR head. Prior to the measurements, the diluents were evaporated from the samples under reduced pressure and dried in a vacuum drier at 55 °C for 30 h. CW-EPR spectra were recorded at room temperature with a Bruker ELEXSYS X-band spectrometer using a rectangular TE102 cavity with the 100 kHz field modulation. The microwave power of 1 mW and the modulation amplitude of 0.5 mT were applied. UV–vis spectra were recorded using an Agilent Technologies Cary 60 spectrophotometer in a range of 200–1000 nm. For spectroscopic measurements, the samples were diluted in heptane (pure, POCH).

Transmission electron microscopy (TEM) observations were carried out using a Tecnai Osiris instrument (FEI) with X-FEG Schottky field emitter operated at an accelerating voltage of 200 kV to evaluate the fuel borne catalyst nanoparticles. Samples for bright field TEM and selected area diffraction (SAED) characterization were prepared by drop-coating organic suspensions onto a lacey carbon-coated Cu grids, then dried at room temperature. The SAED patterns were acquired in order to perform phase analysis of the FBC precursors. Quantitative assessment of the nanoparticle size distribution was performed using an automated analysis method (Digital Micrograph, Gatan) applied to the TEM images. The size histograms were obtained by analysis of c.a. 1800, 1700 and 950 individual particles for FBC-C11, FBC-C18 and FBC-(C11 + C18), respectively.

1.3. Soot oxidation tests

The investigated FBC catalysts are dedicated for light oil burner applications where the nanometric soot particles are produced as an undesired harmful by-product. For model laboratory evaluation of the catalyst performance, following previous literature [12], we used a standard Printex U soot mixed with the FBC catalyst. The temperature-programmed oxidation of Printex U soot (particle size 25 nm, specific surface area 100 $m^2 g^{-1}$, with the volatiles content of 4–5 wt.%, additional characteristics can be found in [27]) was performed on a Mettler Toledo TGA/DSC1 using thermogravimetric and differential thermal analyses (TG/DTA) methods. The experiments were conducted under an air atmosphere (air flow 40 ml/min + purge Ar 20 ml/min) at a temperature ramp of 10 °C/min in the range from room temperature to at least 700 °C.

The reaction mixtures (catalyst-soot) were prepared by mixing the iron-containing residue and soot with a wide mass ratio varying from 8:1 to 1:3. For comparison between the various FBC catalysts the volumetric ratio of 1:1 was used, corresponding to the mass ratio of 8:1. The iron-containing residue was obtained by drying the FBC suspension at ambient conditions. To obtain a *tight contact*, the catalyst and soot particles were ground in an agate mortar for 10 min. In each measurement, ~7 mg of the sample (soot and catalyst mixture) was put in an alumina crucible. As a reference, each FBC catalyst without soot was also investigated for the mass loss in the reaction temperature range to ensure that the observed mass changes can be associated with the soot oxidation process

exclusively. The tests were repeated *de novo* for selected samples up to three times to ensure repeatability of the experiments. The characteristic temperature of the heat flow maximum due to soot oxidation was used as a descriptor of the catalysts activity. Since the soot oxidation is highly exothermic the maximum of the heat flow curve (W = J/s) reflects the very nature of the combustion process more adequately than an arbitrary $T_{50\%}$ or $T_{10\%}$. It was verified that this parameter correlates well with the activation energy of the oxidation process.

2. Results and discussion

The reactivity tests of soot combustion performed with the synthesized FBC catalysts from different precursors are summarized in Fig. 1, together with the oxidation profiles of the FBC catalysts alone. All of the used catalysts decrease remarkably the temperature window of soot oxidation (black curves) in comparison with the non-catalyzed process. Since, as shown below, the size of the iron-oxide cores are similar in all cases the observed differences in soot combustion activity are apparently not associated with the mineral part of the FBC catalyst. The effect depends on the length of the hydrocarbon chain of the carboxylic acid in a pronounced way. The reactivity increases when passing from FBC-C4 to FBC-C18, reaching a maximum for FBC-C18, and decreasing for the capping agent of the chain length of C22. The soot oxidation heat transfer curve for the non-catalyzed reaction is roughly mono-modal and symmetric. In contrast, the addition of the FBC catalysts leads to the appearance of new local maxima on the heat flow curve. This effect may be related to the thermal oxidation/decomposition of the organic capping agents as it can be inferred from the corresponding combustion profiles for the FBC catalysts alone (Fig. 1, grey curves). It was found to depend on the FBC catalyst/soot ratio (vide infra) and the actual mingling state (number of mutual contacts), which is difficult to control, therefore, it is rather poorly reproducible. They are, however, of side importance in the context of this study, and essentially do not influence the main picture conveyed by the obtained results. From the inspection of Fig. 1, it can be deduced that the observed overlapping of the heat flow curves for the FBC catalysts and the soot combustion is correlated with the decrease of the soot combustion temperature. This can be explained assuming that the ignition of the soot particles is initiated by the heat transfer generated by the prior burning of the FBC hydrocarbon tails, taking place at distinctly lower temperatures. The better the overlap between both combustion profiles, the more beneficial the observed effect is, and the shift of the soot combustion to lower temperature is higher. Otherwise, the heat generated during the combustion of the FBC organic component is dissipated and the beneficial ignition effect is diminished.

For the most active FBC-C18 catalyst we have analyzed the soot/FBC catalyst ratio in a wide range, from 8:1 to 1:3 (Fig. 2). It is worth mentioning that the persistent improvement of the activity takes place till the 1:1 mass ratio, which corresponds by volume to ca. 1 part of catalyst per 10 parts of soot. However, in the case of 1:3 mass ratio (1:25 by volume), in addition to spurious pre-peaks discussed above, a clear bimodal combustion profile was observed, indicating that a part of the soot particles burns in a non-catalytic way, apparently because of the lack of the contact with the FBC catalyst.

From the inspection of Fig. 1 it may be noted that in the case of FBC-C11 the combustion temperature is the lowest, whereas for FBC-C18 the overlap of the both oxidation profiles of the catalyst alone and catalyst with the soot is the best. In order to exploit a possible synergy between the preferential FBC catalyst ignition and the optimal heat transfer effect a hybrid catalyst containing simultaneously the C11 and C18 carboxylic acids as the capping agents

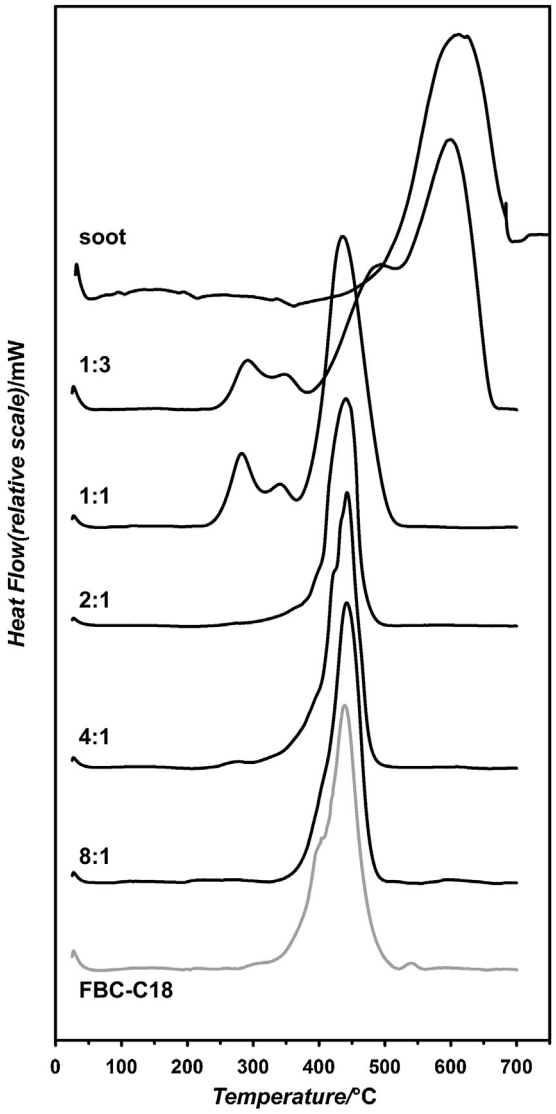

Fig. 2. Reactivity tests of soot combustion performed with the FBC-C18 catalyst with various catalyst/soot ratios (FBC-C18: Printex U).

were synthesized. The soot combustion results for the hybrid FBC-(C11 + C18) catalyst are shown in Fig. 3 (black lines) together with the reference profile of the sole catalyst oxidation (grey lines). The results of two totally independent experiments are shown in order to reveal the extent of the experimental spreading. The combination of two organic capping agents (C11 + C18) results in a different soot combustion behavior. The thermal oxidation curve (grey lines) shows two characteristic maxima, with temperatures related to the oxidation of the individual organic acids stabilizing the iron hydroxy-oxide core. The first peak corresponds to the burning of C11, whereas the second one to the C18 tails (see corresponding profiles for the FBC-C11 and FBC-C18 in Fig. 1 as a reference). Since in both cases the amount of the FBC catalyst is the same, the enhancement of the heat flow observed in both peaks can be assigned to the combustion of soot particles. The most important feature of the soot oxidation curve (black lines) in the presence of the FBC-(C11 + C18) catalyst is the very low ignition temperature (~200 °C), comparable to the ignition of the FBC-C11 catalyst alone (Fig. 1). However, in the presence of this catalyst, soot combustion is shifted to a higher temperature, in contrast to FBC-(C11 + C18), in accordance with the anticipated synergistic effect of the C18 hydrocarbon chains. Tentatively, it can be accounted for by

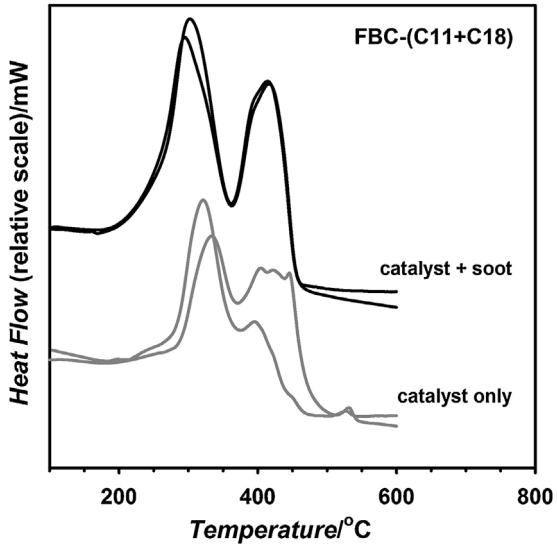

Fig. 3. Reactivity tests of soot combustion, expressed as DTA curves, performed with the FBC-(C11 + C18) precursor (black lines) along thermal decomposition (oxidation) of the FBC catalyst alone (grey lines). Results for two independent measurements are presented.

invoking a more effective penetration/sticking of soot particles by longer chains. It is also worth mentioning that the soot particles burn simultaneously with the organic part of the catalyst, which results in a downshift in the total combustion temperature by 200 °C.

In order to rationalize the observed effect, the FBC catalysts were characterized in both the precursor and final states. The infrared spectra of the investigated samples, presented in Fig. 4, exhibits all the characteristic bands of the carboxylic acids [28]. The broad band spanning from 2500 to 3300 cm^{-1} can be assigned to the O—H stretching mode. The additional band above 3300 cm^{-1} is also due to O—H stretching but related to the iron hydroxide core. Between 2700 and 3000 cm^{-1} there is an intensive group of bands due to symmetric and asymmetric C—H stretching vibrations. Around 1720 cm^{-1} the band due to C=O stretching is clearly visible. The band at 1640 cm^{-1} can be assigned to a C=C stretching mode. A COO— stretching of the acid moiety can be distinguished at 1530 cm^{-1}. Around 1430 cm^{-1} C—O—H in-plane bending, 1240 cm^{-1} C—O stretching, 914 cm^{-1} C—O—H out of plane bending typical bands for carboxylic acids are visible. Among them various methyl, methylene bands are also present. For comparison of the samples we have estimated the relative integrals of the bands due to vibrations of C—H at 2920 cm^{-1} and C=O at 1709 cm^{-1} (only the sharp component), indicated by the gray areas in Fig. 4. The obtained ratios of the peak areas for the FBC-C11, FBC-C18 and FBC-C22 are 2.6, 8.0 and 12.2, respectively. These values are in line with the increasing length of the organic chain. For the FBC-C11 + C18 sample, the same ratio equals to 4.3, which is an average value of the constituting carboxylic acids. This remains in accordance with the assumed 1:1 ratio of the C11 and C18 stabilizers.

In our previous paper, we have shown that the size of the iron oxide particles produced during the combustion of the FBC precursor has a key influence on the soot combustion efficiency [12]. In order to elucidate this issue for the investigated FBC catalysts, we have thoroughly characterized the structure and morphology of the iron core component by means of Raman, UV–vis, EPR and TEM/SAED.

Typical Raman spectra of the investigated materials are shown in Fig. 5. The precursor spectra were obtained for the FBC suspensions dried at a room temperature (25 °C). No particular spectral features can be observed for FBC-C11 sprayed onto a quartz plate,

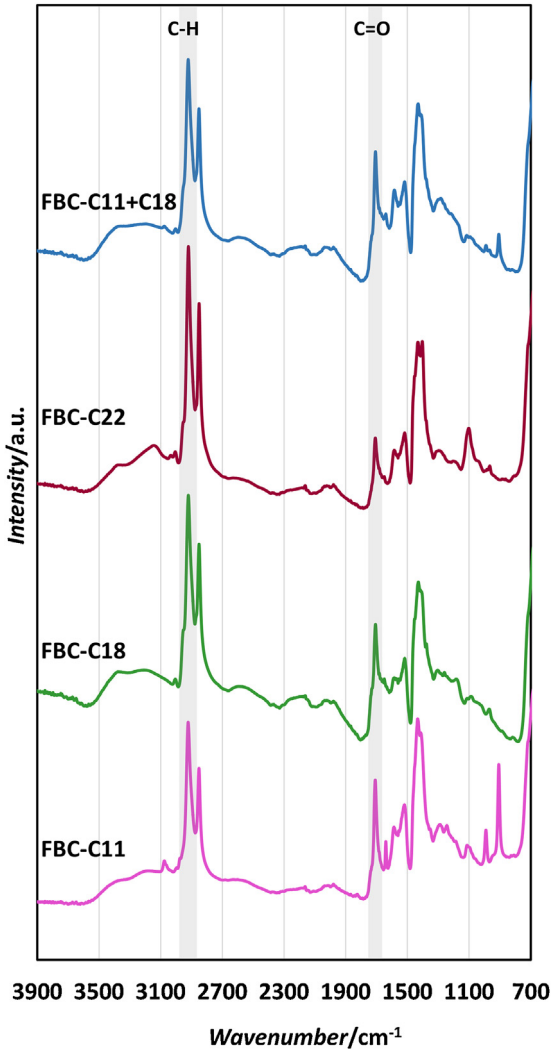

Fig. 4. ATR-FTIR spectroscopic characterization of FBC-C11, FBC-18, FBC-C22 and FBC-(C11 + C18) FBC precursors. Grey areas denote C—H and C=O bands used for calculation of the areas for comparison of the samples.

possibly due to the low intensity of the corresponding bands. However, when the FBC-C11 sample was scraped and piled on a plate, a RS spectrum typical for maghemite was observed with broad bands around 380, 500 and 690 cm^{-1} (▲) [29]. The FBC-C18 and FBC-(C11 + C18) samples exhibit similar maghemite spectra already for the FBC precursors sprayed onto a quartz plate. This higher intensity of the spectra may result from a better crystallinity of the iron oxide cores. The Raman characterization was supported by the UV–vis and EPR measurements (Fig. 6A and B). The UV–vis spectra of the FBC precursors shows typical features of finely divided iron hydroxy/oxide (Fig. 6A), in-line with the Raman data. The maximum at 485 nm is associated with the yellow-reddish color of the aggregated iron oxide clusters in the FBC suspension [30,31], and the intensive absorption below 400 nm to the metal to oxygen charge transfer transition. The corroborative EPR spectra (Fig. 6B) consist of two superimposed signals: a broad at g_{av} = 2.1 (ΔB = 800 G) and a narrow one at g_{av} = 2.0 (ΔB = 40–60 G). The signal at 2.1 can be attributed to Fe^{3+} hydroxy/oxide core broadened by zero field splitting spreading and dipolar interactions. The signal at g_{av} = 2.0 is narrowed by exchange interactions implying the presence of mixed valence iron oxide compacted clusters [32]. It suggests that within the FBC cores magnetite- and maghemite-like domains may coexist. The nanomagnetite, however, can be

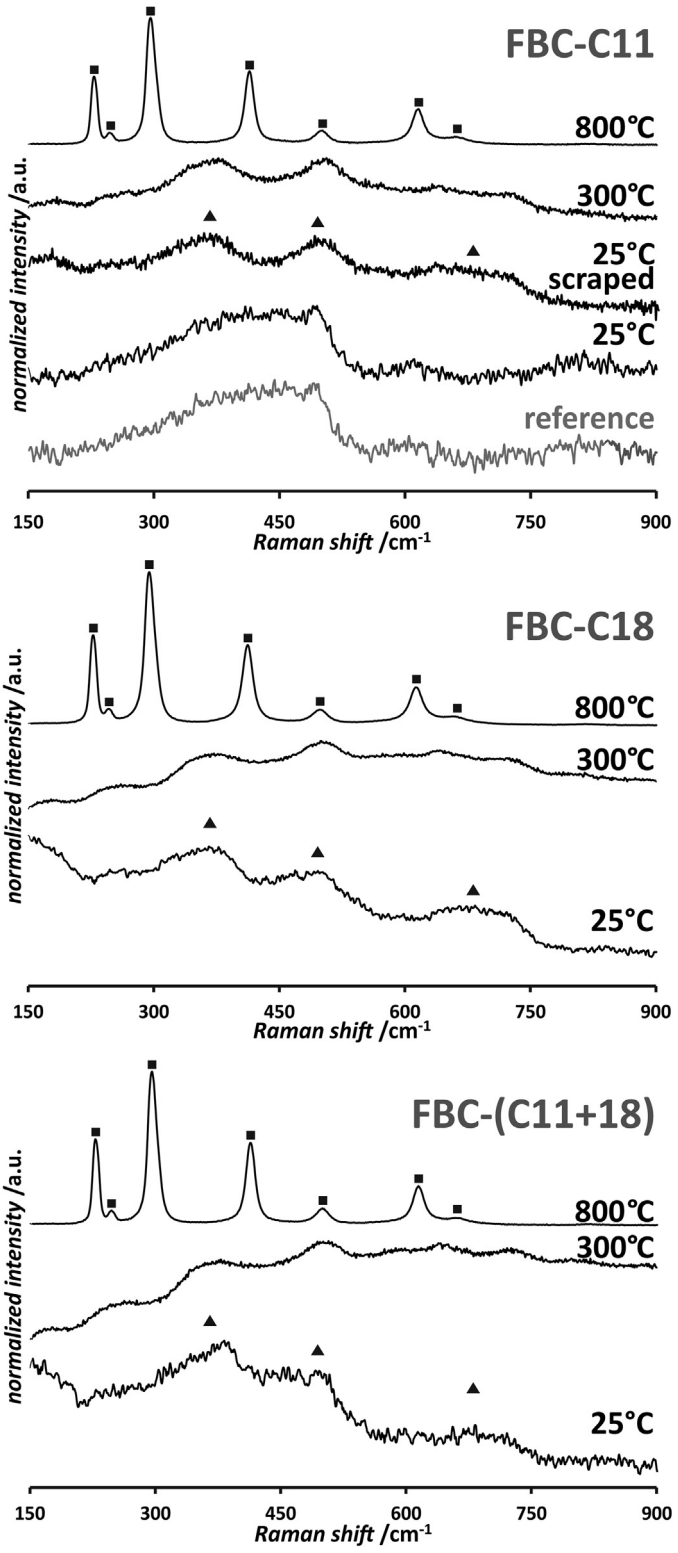

Fig. 5. Raman spectroscopic characterization of FBC-C11, FBC-18 and FBC-(C11 + C18) FBC precursors at room temperature (25 °C), flash calcined at 300 °C and 800 °C. The observed bands designated as squares (■) are due to the hematite while those designated as triangles (▲) are due to the maghemite vibrations.

easily oxidized into maghemite and hematite as recently shown in [33], and rationalized by means of size-dependent thermodynamic diagram of iron-oxide stability at various conditions (temperature and oxygen pressure). So, the coexistence of these sister iron oxide forms is chemically quite labile. The spectroscopic results show that regardless the length of the organic chains of the capping agents the iron-oxide cores are essentially similar in their chemical nature. This point is further examined by Raman and TEM/SAED techniques.

Upon the treatment at intermediate temperatures (300 °C, 4 min in air), the structure of the FBC precursor remained essentially unchanged, still exhibiting Raman bands typical for maghemite. Only an increase of the signal to noise ratio can be observed, probably due to the formation of a better-defined material, caused by the heat treatment and removal of some structural water. To investigate the structure of the final form of the fuel borne catalyst a flash calcination of the precursor was performed prior the Raman spectra recording. Flash calcined samples were prepared by introducing a quartz glass sprayed with the FBC suspension into a furnace preheated to 800 °C for 4 min. The Raman spectra of the flash calcined FBC precursor exhibit several peaks in the range of 150–700 cm^{-1}, with the maxima at 226, 245, 293 and 300 (visible as one band), 411, 496, 612 cm^{-1} and a Raman forbidden mode at 657 cm^{-1} (■). The observed bands can be assigned to the excitations of the structural vibrations of hematite: A_{1g}, $3xE_g$, A_{1g} E_g and E_u, respectively [29]. The overall picture revealed by Raman studies shows again that the chemical nature of the iron core is practically not dependent on the capping agent hydrocarbon chains. In all cases, an amorphous oxo/hydroxo complex present in the FBC precursor transformed into magnetite/maghemite – both of spinel structure. At higher temperatures, typical for burners, maghemite (γ-Fe_2O_3) is readily transformed into a more stable, well-crystalized nano-hematite (α-Fe_2O_3). A more in-depth characterization of such iron oxide nanoparticles was obtained by means of HR-TEM.

The morphology and the phase composition of the iron oxide core of the FBC catalysts, together with the particle size and its distribution, were characterized using bright field TEM observations. Fig. 7 presents TEM images of the FBC-C11 (A), FBC-C18 (B), and FBC-(C11 + C18) (C) catalyst nanocrystals, particle size histograms and the corresponding SAED patterns. The TEM images reveal the presence of rounded grains of the mean diameter around 6–8 nm that tend to form small agglomerates. The equivalent particle diameters were determined by automatic tracking of the maximum radius of quasi-circular particles in TEM images using Digital Micrograph software [34]. The FBC-C11 particles are more of an equant shape and size (Fig. 7A). Their monodisperse histogram can be described by a normal (Gaussian) distribution slightly skewed to the left, with a mean particle size of 5.6 ± 2.1 nm. The more regular and rounded FBC-C18 particles (Fig. 7B) with a log-normal distribution were statistically larger (6.9 ± 2.6 nm). In the case of FBC-(C18 + C11), where the undecylenic and oleic acids were simultaneously used as capping agents, two distinct types of the iron oxide particles (equant and elongated) can be distinguished (Fig. 7C). As a result, the log-normal particle size distribution is broader with the mean value of 7.5 ± 4.2 nm, due to the presence of nanorods with a higher aspect ratio.

The acquired SAED polycrystalline ring patterns of the FBC catalyst (Fig. 7, right panels) were integrated into intensity distributions and presented as a function of the scattering angle using Process Diffraction software [35]. A nonlinear background of electron diffractograms was removed in order to facilitate the assessment of the peak positions in terms of relative peak intensities and the corresponding *d*-values. The calculated kinematic electron diffracted intensities of the maghemite, magnetite and hematite crystallographic structures were marked as a reference. While the phase analysis can rule out the presence of α-Fe_2O_3 on the basis of its

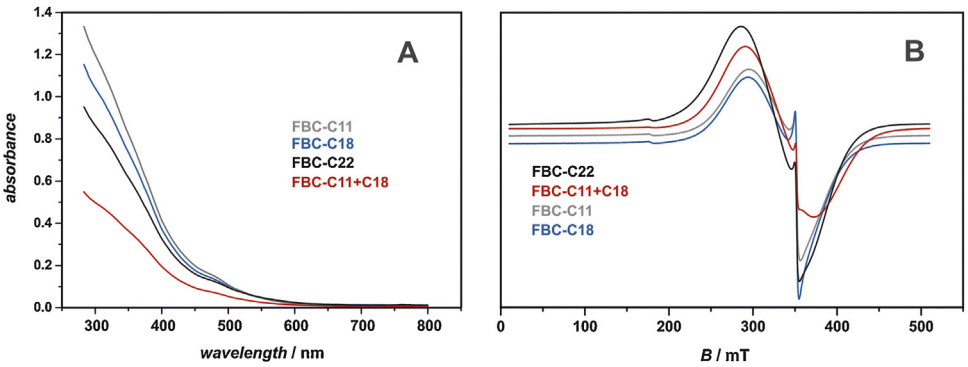

Fig. 6. UV–vis (A) and EPR (B) spectra of the FBC-C11, FBC-18, FBC-C22 and FBC-(C11 + C18) FBC precursors. (For interpretation of the references to colour in this figure legend, the reader is referred to the web version of this article.)

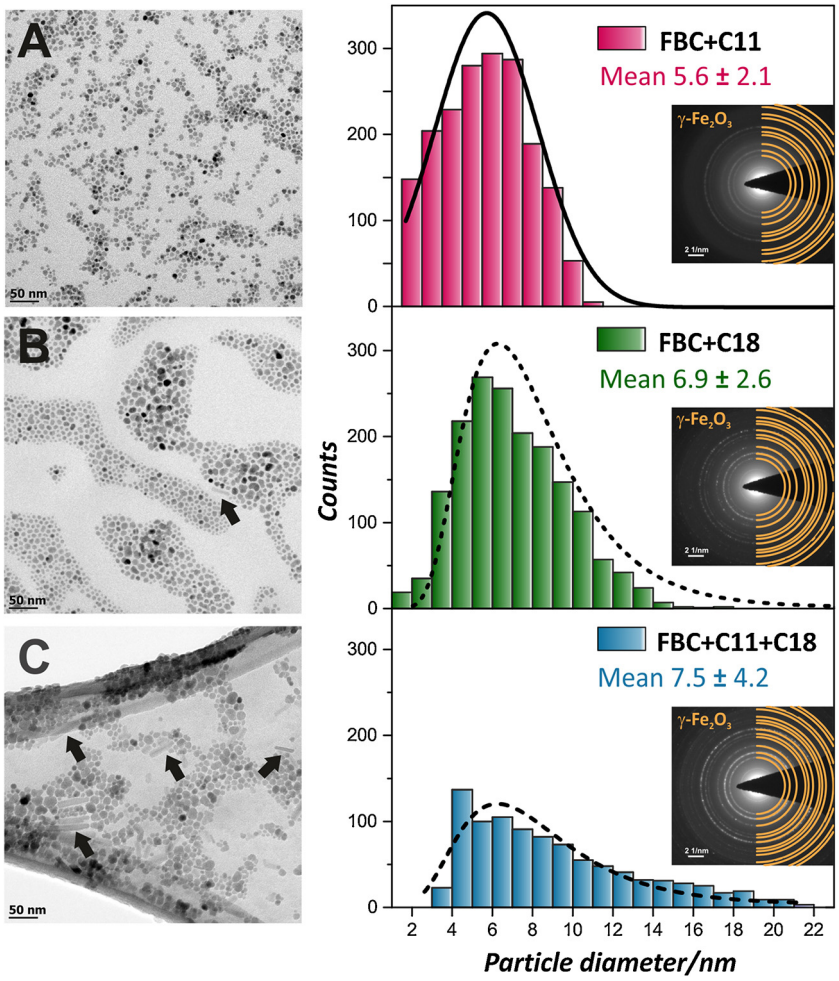

Fig. 7. Bright field TEM images of FBC precursors FBC-C11, FBC-C18, FBC-(C11 + C18) along with particle size distributions and selected area electron diffraction patterns. The position of detected and indexed diffraction rings of the spinel structure is shown.

different lattice parameters (Fig. 8), the distinction between the two spinel structures of iron oxide magnetite (Fe_3O_4) and maghemite (γ-Fe_2O_3) is not univocal, mainly due to the nanoparticle size broadening of the diffraction lines. However, by taking advantage of the small size of the average FBC particles (below ~10 nm), and a nanoparticle layer of the investigated samples on a carbon support, dynamic effects in the recorded electron diffraction patterns are minimized [36]. Indeed, as can be seen in Fig. 8, the comparison of the relative intensities of the kinematic markers with the integrated experimental SAED intensities suggests the presence of maghemite rather than magnetite phase, regardless the nature of the organic component in the FBC precursors. As already mentioned, the highly defected, unstable γ-Fe_2O_3 can be readily transformed into ordered α-Fe_2O_3 in the process conditions, as shown elsewhere [37].

It has been recently found that the size of the iron oxide particles plays a crucial role for their catalytic soot oxidation activity [12]. The beneficial effect is observed for the particles below 100 nm in size with the best performance for particles of 5–15 nm. Both the investigated FBC catalysts, as well as the particles accumulated at the end-pipe filter, when FBC additives are used, show uniformly

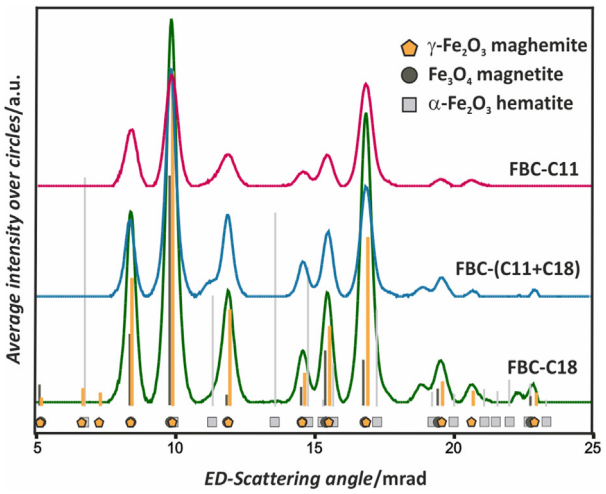

Fig. 8. Electron diffraction phase analysis confirming the maghemite phase of the FBC precursors. Comparison of radially integrated intensities of ED patterns shown in Fig. 7 as a function of the scattering angle; FBC-C11 (red), FBC-C18 (green), and FBC-C11 + C18 (blue). For clarity, vertical markers indicate positions of different crystallographic phases: maghemite (yellow; pentagon), magnetite (black; circle), and hematite (gray; square). (For interpretation of the references to colour in this figure legend, the reader is referred to the web version of this article.)

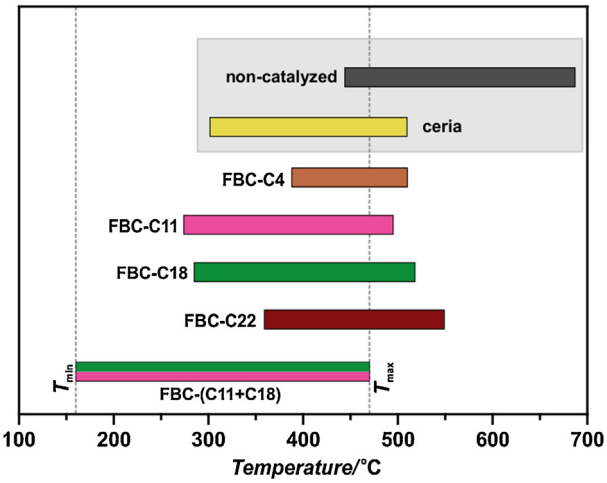

Fig. 9. Summary of temperature windows for soot oxidation in the presence of FBC precursors along with some iron-based common active catalytic materials and CeO_2. (For interpretation of the references to colour in the text, the reader is referred to the web version of this article.)

dispersed iron oxide nanocrystals with the size in the catalytically favorable range. Therefore, all the observed differences in the soot oxidation performance of the investigated FBC catalysts can, consistently, be associated with the nature of the organic component.

It is worth mentioning that in the real condition process the amount of soot collected is by 50% lower when FBC catalyst was added (CH_x, CO, and NO_x emissions were reduced by 85%, 70% and 5%, respectively) as reported in [38]. This shows clearly that even in the real conditions the effect of the FBC catalyst is not overcompensated by the presence of the fuel hydrocarbons. This implies that the contact between the hydrocarbon and the iron-oxide core is crucial for accounting of the observed effect of the capping agent tail lengths.

The temperature windows of the soot oxidation reactions presented in Figs. 1 and 3 are summarized in Fig. 9. It shows the reactivity of the iron oxide core of various FBC catalysts with different organic capping molecules. For the sake of convenience, the temperature ranges of non-catalyzed soot oxidation (black bar) and a ceria reference catalyst (yellow bar) are also indicated. The catalytic data for ceria was taken from the reference [39], where similar experimental conditions were used (*tight contact* and Printex U). In all cases the beneficial role of the FBC catalyst is apparent. However, the best results (delineated by T_{min} and T_{max} dashed lines) are observed for the FBC-(C11 + C18) hybrid catalyst, for which the ignition temperature is lowered to almost 150 °C and the total soot combustion is accomplished below ~470 °C. Such a spectacular effect of two different (short C11 and long C18) capping agents can be discussed in terms of the ignition boosting (C11) and maximal overlapping of the heat transfer from the long tail component (C18) to soot particles. It is worth emphasizing here, that the observed substantial lowering of the soot combustion temperature overwhelms the effect of the iron-oxide particle size. For Fe_2O_3 of the same nanoparticles size in similar conditions, soot oxidation requires at least 600 °C for complete combustion by the most active catalyst. We may thus conclude that the exceptional activity of the hybrid FBC catalysts, related with the presence of two capping agents with different hydrocarbons chain lengths, makes the fuel borne catalyst a promising alternative/backup for the current active soot particle filter technology. The obtained results also suggest that in soot combustion the native hydrocarbon components may play an important role in the ignition of real soot. It should be noted, however, that although such conjecture accounts well for the observed phenomenon, the actual relevance of the observed heat transfer between the catalysts and the soot particles should be further investigated in more detail for its definite justification.

3. Conclusions

Fuel borne catalysts based on an iron oxide core stabilized by various long chain methacrylic (C4), undecylenic (C11), oleic (C18) and erucic (C22) carboxylic acids are highly active in soot combustion, lowering the reaction temperature window from 500 to 700 °C (bare soot) to 300–500 °C. The TEM observations revealed that the core of the catalyst consists of Fe_2O_3 of a crystallite size in the beneficial range of 6–8 nm, regardless of the nature of the capping agent. The highest activity was obtained for the hybrid FBC catalyst with the simultaneous presence of two types (C11 and C18) of the capping ligands. For this catalyst, the ignition temperature of soot combustion was lowered to almost 150 °C and the total soot combustion accomplished below ~470 °C. The effect of two different (short C11 and long C18) capping agents was discussed in terms of the proposed ignition boosting (C11) and maximal overlapping of the heat transfer from the long tail component (C18) to soot particles. The high activity of the hybrid FBC catalysts, makes them as a promising alternative/backup for the current active soot particle filter technology.

Acknowledgements

The authors would like to acknowledge the Polish National Centre for Research and Development funding awarded by the decision number PBS1/B1/4/2012.

The research was carried out with the equipment purchased thanks to the financial support of the European Regional Development Fund in the framework of the Polish Innovation Economy Operational Program (contract no. POIG.02.01.00-12-023/08).

Appendix A. Supplementary data

Supplementary data associated with this article can be found, in the online version, at http://dx.doi.org/10.1016/j.apcatb.2016.06.056.

References

[1] Commission Regulation (EU) No 459/2012 with Amendments to Regulation (EC) No 715/2007.
[2] N.K. Gurusala, V.A.M. Selvan, Clean Technol. Environ. 17 (2015) 681–692.
[3] H. Zhao, Y. Ge, T. Zhang, J. Zhang, J. Tan, H. Zhang, J. Environ. Sci. 26 (2014) 2027–2033.
[4] J. Song, J. Wang, A.L. Boehman, Combust. Flame 146 (2006) 73–84.
[5] N.V. Heeb, P. Schmid, M. Kohler, E. Gujer, M. Zennegg, D. Wenger, A. Wichser, A. Ulrich, U. Gfeller, P. Honegger, K. Zeyer, L. Emmenegger, J.L. Petermann, J. Czerwinski, T. Mosimann, M. Kasper, A. Mayer, Environ. Sci. Technol. 42 (2008) 3773–3779.
[6] A. Liati, P. Dimopoulos Eggenschwiler, E. Müller Gubler, D. Schreiber, M. Aguirre, Atmos. Environ. 49 (2012) 391–402.
[7] Z.-H. Zhang, R. Balasubramanian, Appl. Energy 146 (2015) 270–278.
[8] M. Zhu, Y. Ma, D. Zhang, Appl. Energy 91 (2012) 166–172.
[9] M. Zhu, Y. Ma, D. Zhang, Appl. Energy 102 (2013) 556–562.
[10] M. Zhu, Y. Ma, D. Zhang, Appl. Energy 113 (2014) 751–757.
[11] F. Zasada, W. Piskorz, P. Stelmachowski, P. Legutko, A. Kotarba, Z. Sojka, J. Phys. Chem. C 119 (2015) 6568–6580.
[12] P. Stelmachowski, A. Kopacz, P. Legutko, P. Indyka, M. Wojtasik, L. Ziemiański, G. Żak, Z. Sojka, A. Kotarba, Catal. Today 257 (2015) 111–116.
[13] S. Wagloehner, S. Kureti, Appl. Catal. B: Environ. 125 (2012) 158–165.
[14] S. Wagloehner, S. Kureti, Appl. Catal. B: Environ. 129 (2013) 501–508.
[15] S. Wagloehner, J.N. Baer, S. Kureti, Appl. Catal. B: Environ. 147 (2014) 1000–1008.
[16] D.G. Nash, N.B. Swanson, W.T. Preston, T.L.B. Yelverton, W.L. Roberts, J.O.L. Wendt, W.P. Linak, J. Aerosol Sci. 58 (2013) 50–61.
[17] G.R. Kannan, R. Karvembu, R. Anand, Appl. Energy 88 (2011) 3694–3703.
[18] D. Lee, J.Y. Sung, J.H. Park, Y. Hong, S.H. Lee, S. Oh, K. Lee, Catal. Today 157 (2010) 432–435.
[19] T. Okuda, J. Schauer, M. Olson, M. Shafer, A. Rutter, K. Walz, P. Morschauser, Energy Fuels 23 (2009) 4874–4980.
[20] S. Steiner, J. Czerwinski, P. Comte, N.V. Heeb, A. Mayer, A. Petri-Fink, B. Rothen-Rutishauser, Anal. Bioanal. Chem. 407 (2015) 5977–5986.
[21] P. Legutko, P. Stelmachowski, M. Trębala, Z. Sojka, A. Kotarba, Top. Catal. 56 (2013) 489–492.
[22] P. Legutko, W. Kaspera, T. Jakubek, P. Stelmachowski, A. Kotarba, Top. Catal. 56 (2013) 745–749.
[23] H. Bladt, J. Schmid, E.D. Kireeva, O.B. Popovicheva, N.M. Perseantseva, M.A. Timofeev, K. Heister, J. Uihlein, N.P. Ivleva, R. Niessner, Aerosol Sci. Technol. 46 (2012) 1337–1348.
[24] M.E. Gálvez, S. Ascaso, P. Stelmachowski, P. Legutko, A. Kotarba, R. Moliner, M.J. Lázaro, Appl. Catal. B: Environ. 152–153 (2014) 88–98.
[25] M.V. Kovalenko, M.I. Bodnarchuk, R.T. Lechner, G. Hesser, F. Schäffler, W. Heiss, J. Am. Chem. Soc. 129 (2007) 6352–6353.
[26] D. Zhang, Y. Ma, M. Zhu, Proc. Combust. Inst. 34 (2013) 1869–1876.
[27] http://www.oecliterature.com/pdf/OEC-3130-carbonblackpolymersamerica.pdf (accessed: 13.10.15).
[28] B. Stuart, Infrared Spectroscopy: Fundamentals and Applications, John Wiley & Sons, Ltd., 2004.
[29] D.L.A. de Faria, S.V. Silva, M.T. de Oliveira, J. Raman Spectrosc. 28 (1997), 878–878.
[30] D. Macina, Z. Piwowarska, K. Góra-Marek, K. Tarach, M. Rutkowska, V. Girman, A. Błachowski, L. Chmielarz, Mater. Res. Bull. 78 (2016) 72–82.
[31] Y. Ohishi, T. Kawabata, T. Shishido, K. Takaki, Q. Zhang, Y. Wang, K. Nomura, K. Takehira, Appl. Catal. A: Gen. 288 (2005) 220–231.
[32] F.E. Mabbs, D. Collison, Electron Paramagnetic Resonance of D Transition Metal Compounds, Elsevier, 1992.
[33] J. Kaczmarczyk, F. Zasada, J. Janas, P. Indyka, W. Piskorz, A. Kotarba, Z. Sojka, ACS Catal. 6 (2016) 1235–1246.
[34] H.G. Merkus, Particle Size Measurements – Fundamentals, Practice, Quality, Springer, Netherlands, 2009, pp. 29–30.
[35] J.L. Lábár, Microsc. Microanal. 18 (2012) 406–420.
[36] J.L. Weirich, Electron Crystallography Novel Approaches for Structure Determination of Nanosized Materials, Springer, Netherlands, 2006, pp. 215–217 (355).
[37] L. Machala, J. Tucek, Radek Zboril, Chem. Mater. 23 (2011) 3255–3272.
[38] P. Stelmachowski, A. Kopacz, T. Jakubek, P. Indyka, J. Markowski, M. Wojtasik, L. Ziemiański, W. Krasodomski, G. Żak, Z. Sojka, A. Kotarba, Top. Catal. (2016), http://dx.doi.org/10.1007/s11244-016-0625-8.
[39] M. Piumetti, S. Bensaid, N. Russo, D. Fino, Appl. Catal. B: Environ. 165 (2015) 742–751.